NANO LETTERS

Letter

pubs.acs.org/NanoLett

Delayed Exciton Emission and Its Relation to Blinking in CdSe Quantum Dots

Freddy T. Rabouw,[†] Marko Kamp,[‡] Relinde J. A. van Dijk-Moes,[†] Daniel R. Gamelin,[§] A. Femius Koenderink,[‡] Andries Meijerink,[†] and Daniël Vanmaekelbergh*[,†]

[†]Condensed Matter and Interfaces, Debye Institute for Nanomaterials Science, Princetonplein 1, 3584 CC Utrecht, The Netherlands

[‡]Center for Nanophotonics, FOM Institute AMOLF, Science Park 104, 1098 XG Amsterdam, The Netherlands

[§]Department of Chemistry, University of Washington, Seattle, Washington 98195-1700, United States

Supporting Information

ABSTRACT: The efficiency and stability of emission from semiconductor nanocrystal quantum dots (QDs) is negatively affected by "blinking" on the single-nanocrystal level, that is, random alternation of bright and dark periods. The time scales of these fluctuations can be as long as many seconds, orders of magnitude longer than typical lifetimes of exciton states in QDs. In this work, we investigate photoluminescence from QDs delayed over microseconds to milliseconds. Our results prove the existence of long-lived charge-separated states in QDs. We study the properties of delayed emission as a direct way to learn about charge carrier separation and recovery of the exciton state. A new microscopic model is developed to connect delayed emission to exciton recombination and blinking from which we conclude that bright periods in blinking are in fact not characterized by uninterrupted optical cycling as often assumed.

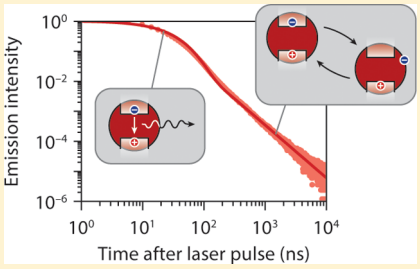

KEYWORDS: *Nanocrystal, colloidal quantum dot, charge carrier trapping, blinking, excited state dynamics*

Blinking, or intermittency, in the photoluminescence (PL) of individual semiconductor nanocrystal quantum dots (QDs) is a fascinating phenomenon that is still not fully understood.[1,2] Soon after the first observation of blinking in individual QDs[3] the idea was proposed that dark periods were due to temporary charging.[4] Charging would render the QD dark because subsequent excitations would decay not by the emission of a photon but by Auger recombination, that is, transfer of the recombination energy to the excess charge carrier. This basic idea has been used to develop detailed models for blinking.[5−7] To explain the characteristic power-law statistics of the durations of bright and dark periods, these models assume that the rates of charging (by charge carrier ejection and trapping) and discharging (by recombination or release of the trapped charge) of the QD fluctuate in time. Recent experimental results have put into question the idea that Auger quenching alone can explain the dark periods.[8−10] They support alternative blinking models, where the dark states are due to charge carrier localization and nonradiative recombination on structural defects in the QD.[11−13] It has also been proposed that blinking can be due to a combination of Auger decay and nonradiative recombination at trap sites.[14,15] One of the reasons that there is still not one unifying physical model for blinking is that models are based on rather indirect experimental data, namely the statistics of bright and dark durations.

In this work, we examine the PL dynamics of core−shell CdSe/CdS/CdZnS/ZnS QDs over 10 orders of magnitude in time. There is exciton recombination on the nanosecond time scale and blinking on the second time scale. We focus in particular on "delayed emission" on time scales from microseconds to milliseconds.[16−18] This component in the PL decay dynamics of QDs is often overlooked because, although its integrated intensity can be higher than 10%, the amplitude is much less than a percent of the exciton emission. We examine the properties of delayed emission, concluding that it is due to charge separation, storage, and eventual recovery of the lowest exciton state. Interestingly, the decay of delayed emission follows a power law, very similar to the statistics of bright and dark durations in blinking. A unifying microscopic model is presented to account for both delayed emission and blinking.

Emission Dynamics in Core−Shell Quantum Dots. The QDs investigated have a CdSe/CdS/CdZnS/ZnS core−shell structure with a 3.4 nm diameter CdSe core, and emit around 630 nm (Figure 1a−d). Single-QD spectroscopy illustrates the many different dynamical processes that can occur in a QD. The emission intensity trace (Figure 1e) of a single core−shell QD over a period of 5 min of continued excitation exhibits blinking, that is, on time scales of up to seconds the QD switches randomly between a state of bright emission (blue shaded area) and states of intermediate brightness (green) or near complete darkness (red). The probability distributions for the duration of bright (ON; blue) and dark (OFF; red) periods (Figure. 1f), obtained with a threshold analysis,[5] show that the

Received: September 15, 2015
Revised: October 16, 2015
Published: October 23, 2015

DOI: 10.1021/acs.nanolett.5b03818
Nano Lett. 2015, 15, 7718−7725

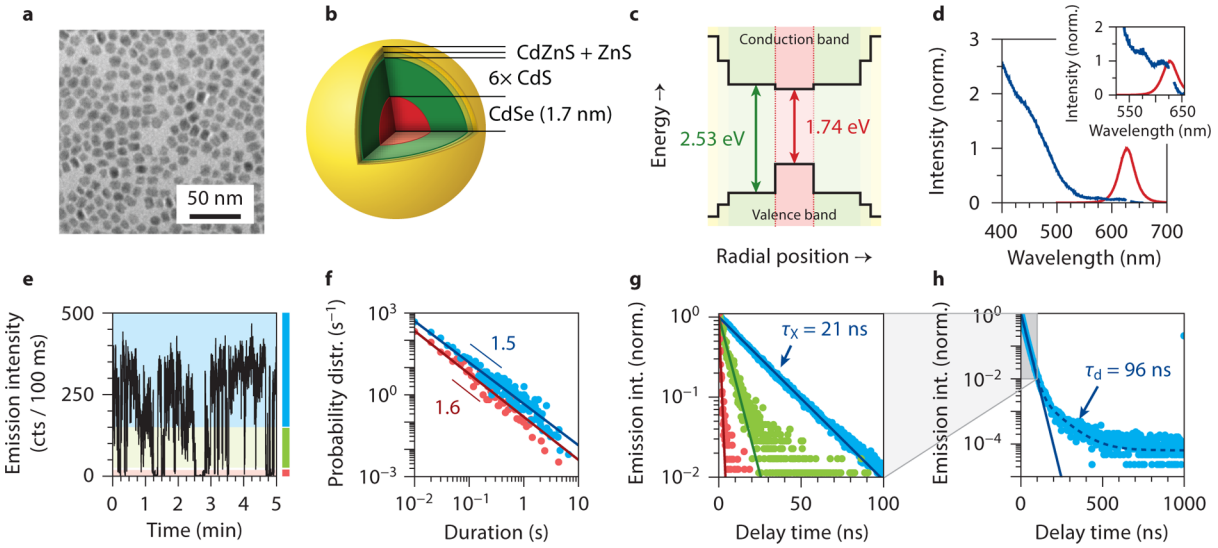

Figure 1. Properties of the core−shell quantum dots investigated. (a) A transmission electron microscopy image of the CdSe/CdS/CdZnS/ZnS core−shell QDs. They have a slightly anisotropic shape of 11.4 ± 1.0 nm by 8.2 ± 0.7 nm (mean ± standard deviation over 100 QDs). (b) A schematic of the QD geometry investigated with a CdSe core of 1.7 nm radius, covered by six monolayers (nominally) of CdS, one monolayer of CdZnS, and one monolayer of ZnS. (c) The band structure diagram of the QDs.[19] Emission originates from the CdSe core with a bulk band gap of 1.74 eV. (d) PL excitation (blue) and emission (red) spectra of the ensemble of QDs. There is a single emission band centered at 630 nm originating from exciton recombination in the CdSe core. The excitation spectrum is dominated by strong absorption by the CdS shell at wavelengths shorter than 500 nm. The inset is a zoom-in, revealing the discrete electronic transitions in the CdSe core. (e) An emission intensity trace of a single core−shell QD under continued excitation. The bin size is 100 ms. Colored shadings indicate the ranges of intensity values that for further analysis are considered bright (blue), intermediate (green), and dark (red). (f) The probability distribution of the duration of bright (blue) and dark (red) periods, extracted from the emission intensity trace at a bin size of 10 ms. Solid lines are fits to a power-law trend, from which we obtain exponents of 1.5 for the bright periods, and 1.6 for the dark periods. (g) PL decay curves of the bright (blue), intermediate (green), and dark (red) periods, constructed after selecting time bins based on emission intensity. Solid lines are fits to single-exponential decay. We obtain the exciton lifetime of τ_X = 21.3 ns from the bright periods, and PL lifetimes of 5.5 and 0.9 ns during the intermediate and dark periods, respectively. With a bin width of 0.165 ns, the absolute peak counts in the PL decay curves are 21.5 (blue), 14.8 (green), and 5.3 (red) cts/100 ms. The lower peak counts during intermediate and dark periods might occur because the fastest decay component is faster than the bin size. (h) PL decay curve for the bright periods plotted over a time range of 1 μs. The solid line is the single-exponential fit to the first 100 ns (with τ_X = 21.3 ns; panel g). Adding a second exponential decay component and a background yields the dashed line. We obtain a time constant for the delayed component of τ_d = 96 ns. This PL decay curve has a bin width of 1.65 ns, 10× wider than in panel g.

time scales of the ON/OFF fluctuations range from 10 ms to several seconds. Solid lines are fits to a power-law distribution ($p(t) = t^{-\alpha}$ with t the duration of a period) that yield α_{ON} = 1.5 and α_{OFF} = 1.6, as typically found for blinking statistics.[2,5,21]

The PL decay curve of this QD during bright periods (blue data points in Figure 1g) is single-exponential over 2 orders of magnitude in intensity with a lifetime of τ_X = 21.3 ns, consistent with the radiative lifetime of the exciton in CdSe QDs. During periods of intermediate intensity (green) or dark periods (red), the PL decay is faster with fitted lifetimes of 5.5 and 0.9 ns, respectively. Such fast decay dynamics are due to nonradiative decay pathways, which have previously been interpreted as Auger recombination of a trion state[4,22−24] or rapid charge carrier trapping on nonradiative recombination centers[8,10,11] (see below for further discussion). In Supporting Information Figure S5, we show that, as reported before,[12] the precise values for the power exponents extracted as well as the PL lifetimes fitted depend (slightly) on the thresholds chosen in the analysis.

Clearly, a remarkably wide range of time scales is involved in the emission characteristics of QDs. On the one hand there is the time scale of nanoseconds on which excitations decay (Figure 1g), while on the other hand there is the time scale of milliseconds to seconds on which the emission intensity fluctuates (Figure 1f). There are a few papers[16,17] discussing "delayed" PL from CdSe QDs on the time scale of up to 1−10 μs. Another paper has reported delayed emission in Cu^+-doped CdSe QDs on time scales of >10 ms at room temperature and up to 1 s at cryogenic temperatures.[18] Indeed, on time scales beyond 100 ns the PL decay curve of the bright state in our single QD (Figure 1f) deviates from the single exponent with the exciton lifetime of τ_X = 21 ns (solid line). We can add an exponential "delayed component" plus background to the fit (dashed line) and obtain a delayed lifetime of τ_d = 96 ns. The lifetime of this component is too long to originate from direct radiative recombination of an exciton. In analogy to previous papers,[16,17] we ascribe the delayed emission to exciton storage in a charge-separated state for long periods before eventual recovery of the delocalized $1S_{3/2}1S_e$ exciton state (i.e., with band-edge orbitals occupied) and emission. In this charge-separated state, (at least) one charge carrier is trapped on the surface or in the environment of the QD. Charge carrier release leading to QD emission has previously also been investigated using thermoluminescence experiments.[20]

Connecting the Nanosecond and Millisecond Time Scales. To further examine the delayed emission dynamics, we measure the PL decay of the QD ensemble when dispersed in toluene. On a 100 ns time scale, the PL decay of the ensemble (Figure 2a) looks similar to that of the single QD discussed above. At delay times longer than 100 ns the decay curve (Figure 2b) deviates from the double-exponential fit of Figure 2a (dot-dashed line). In fact, the PL decay follows a power-law

DOI: 10.1021/acs.nanolett.5b03818
Nano Lett. 2015, 15, 7718−7725

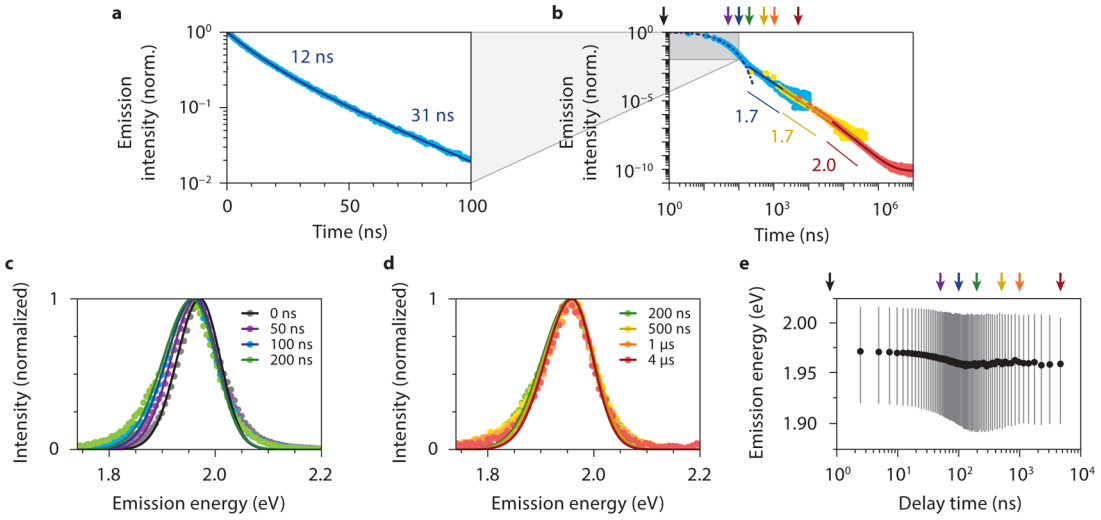

Figure 2. Delayed emission after up to milliseconds. (a) The ensemble PL decay curve of the core−shell QDs appears near exponential on a 100 ns time scale. A biexponential fit yields lifetime components of 12 and 31 ns. (b) We can measure PL from the ensemble of QDs until up to as long as milliseconds after the laser pulse. On time scales longer than 100 ns the PL decay clearly deviates from the biexponential behavior (blue dash-dotted line) fitted to the first 100 ns. Blue, yellow, and red data points are three separate measurements, taken with a diode laser with a repetition rate of 100 kHz (blue), an OPO laser with a repetition rate of 20 Hz (yellow, red). The red curve was taken on a concentrated QD dispersion over a measurement time of 3 days. The PL decay after a delay time of 200 ns can be fitted to power-law decay, yielding a power exponent of 1.7 between 200 ns and 400 μs, and 2.0 between 50 μs and 5 ms. (c) The emission spectrum of the ensemble of QDs in toluene at varying time delays after the excitation pulse of 0 (black), 50 (purple), 100 (blue), and 200 (green) ns. The emission peak redshifts over 15 meV and the spectrum becomes broader by 20 meV. The solid lines are fits to a two-sided Gaussian (see Methods). (d) The emission spectrum at longer delay times of 200 (green; same as in panel c), 500 (yellow), 1000 (orange), and 4000 (red) ns. The changes occurring in the first 200 ns are partially reversed: the peak blueshifts over 2 meV, and the bandwidth decreases by 10 meV. (e) The emission energy (dots) and bandwidth (lines) of the ensemble of QDs as a function of delay time after the excitation pulse, as obtained from two-sided Gaussian fits to the emission spectra (see Methods). Arrows on the top mark the spectra shown in panels c and d.

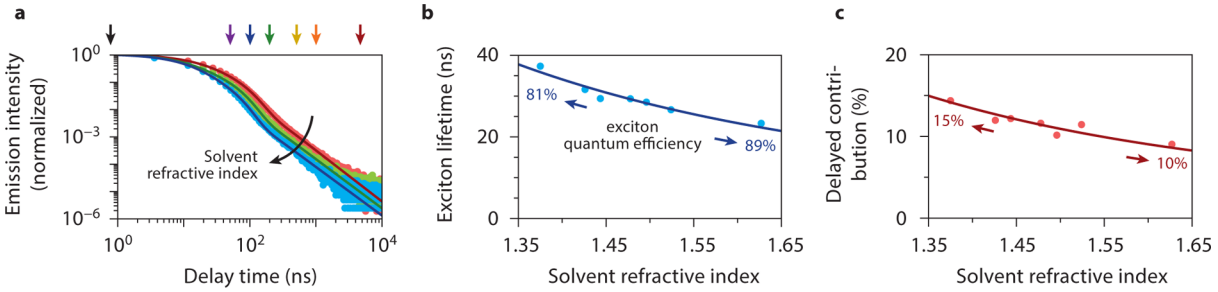

Figure 3. Photonic effects on charge carrier trapping. (a) PL decay curves of the ensemble of QDs over a time scale of 10 μs for different solvents in which they are dispersed: hexane (red; refractive index n = 1.375), trichloroethylene (green; n = 1.478), and carbon disulfide (blue; n = 1.627). Solid lines are fits to decay with a biexponential contribution from direct exciton recombination and a power-law contribution from delayed emission. Arrows on the top mark the delay times for which the spectra are shown in Figure 2c,d. (b) The exciton lifetime [average lifetime from a biexponential fit to the first 100 ns of decay (see Figure 2a), weighted by integrated intensity] is shorter in solvents with higher refractive index, because the local density of optical states is higher.[29] From the data, we fit that the quantum efficiency of the exciton, that is, the probability of direct radiative decay, is roughly 80−90% depending on the refractive index. (c) The contribution of power-law delayed emission as a percentage of the total number of photons emitted, as obtained from a fit to eq 2. The presence of a trend with solvent refractive index indicates that charge carrier separation happens from the lowest exciton state and competes with direct radiative recombination of the exciton. The solid line is a fit assuming that the rate of charge separation is fixed, while the rate of radiative decay of the exciton changes with the local density of optical states.[31]

over the next 4 orders of magnitude in time (from ∼100 ns to 1 ms) and 7 orders of magnitude in emission intensity. The power exponents that we fit are similar to those of the blinking statistics (Figure 1d), namely 1.7 between 200 ns and 400 μs, and 2.0 between 50 μs and 5 ms. Interestingly, the integrated intensity of delayed emission contributes as much as 10−15% of the total number of emitted photons. This would mean that following excitation there is at least a 10−15% probability of charge separation. The observation of delayed emission from several single QDs (Supporting Information, Figure S2)[16] indicates that the competition between direct and delayed emission happens on the single-QD level, rather than being an ensemble effect.

Figure 2c,d compares the exciton emission and delayed emission spectra of the ensemble of QDs in toluene. In the first 200 ns (Figures 2c) after excitation, the emission peak shifts to the red. This can be explained considering that the rate of radiative decay of the exciton is proportional to the density of optical states. As a result, small QDs emitting at high energies should have faster radiative decay (because the density of optical states is high) than larger ones emitting at lower energy (where the density of optical states is lower).[25−28] The

DOI: 10.1021/acs.nanolett.5b03818
Nano Lett. 2015, 15, 7718−7725

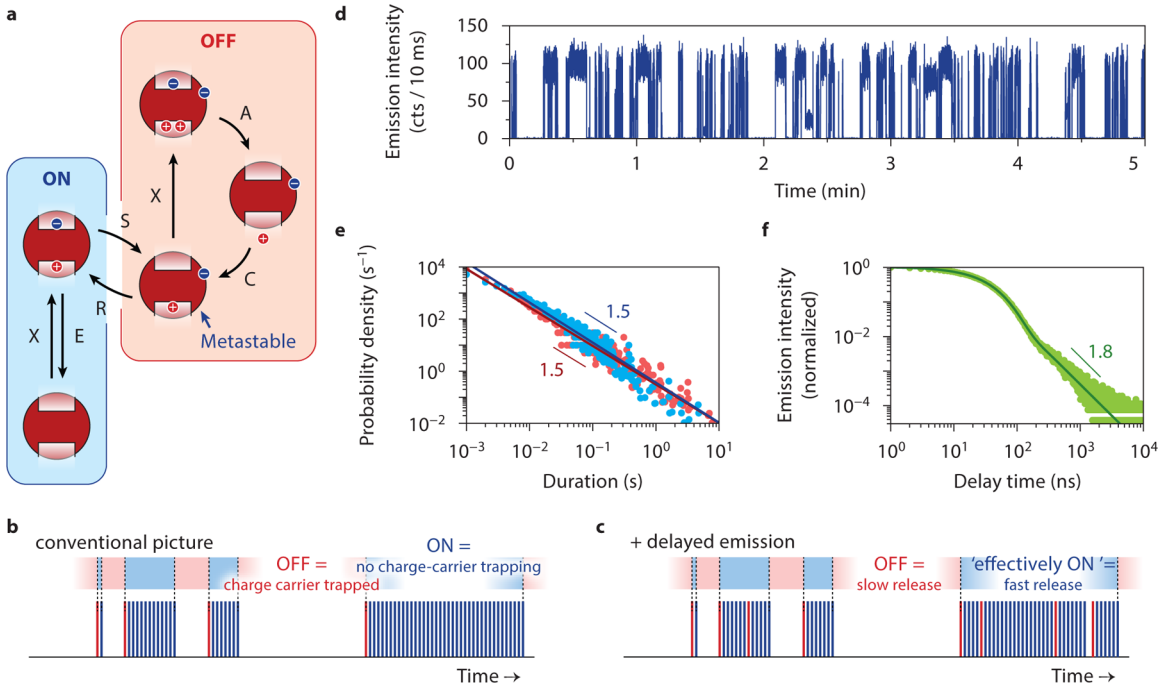

Figure 4. Simulation of power-law delayed emission and power-law blinking. (a) In the charging model for blinking, optical cycling (X, excitation; E, emission) in the ON-state (blue panel) is sometimes interrupted by charge carrier separation (S): ejection of a carrier from the QD core and trapping in the environment, for example, on the surface or in the shell. This leaves the QD with a single delocalized carrier. The QD is then OFF (red panel) because subsequent excitations (X) decay nonradiatively via Auger recombination (A) and charge carrier cooling (C). The QD returns to the ON-state if the delocalized exciton state recovers (R) by release of the trapped carrier. In our model, the probability for charge separation P_S is fixed, while the recovery rate γ_R fluctuates strongly over time (see Methods). (b,c) The difference between existing blinking models and our new model. We plot the photon emission events (blue and red bars) from an individual QD as a function of experiment time under continued excitation. Blue bars are direct photons (i.e., no charge-carrier separation and release), while red bars are delayed photons. While a charge carrier is trapped, the QD is dark (i.e., no photons emitted). In existing models (b), the QD is ON when there is no charge carrier separation for a prolonged period of time. In our new model (c), charge-carrier separation continues during ON periods but the release is fast during a prolonged period. (d) An emission intensity trace simulated with our model for a laser repetition period of 1 μs, an exciton decay rate of $\gamma_X = 1/30$ ns, a probability of charge carrier separation of $P_S = 15\%$, and diffusion and release exponents of $\alpha_D = 1.7$ and $\alpha_R = 1.55$ (see Methods). (e) The durations of bright and dark periods are power-law distributed, although there is a deviation in the bright statistics for durations shorter than 10 ms (blue data points deviate from the blue line). (f) The histogram of delay times shows an exponential component originating from direct exciton recombination and a power-law delayed component. From a fit to eq 2, we obtain a power exponent of $\alpha = 1.8$ and recover the input values of $P_S = 15.4\%$ and $\gamma_X = 1/29.7$ ns.

spectrum of the delayed emission (Figure 2d) is similar to the exciton emission but with the emission peak position slightly redshifted by ~10 meV (see also Figure 2e). From this similarity, we conclude that delayed emission is the result of recovery of and emission from the delocalized $1S_{3/2}1S_e$ exciton state, rather than direct radiative recombination of charge carriers in the charge-separated state. The redshift of ~10 meV of the delayed emission compared to the exciton emission might indicate that in the smaller QDs of the ensemble, that is, those emitting at shorter wavelengths, charge carrier separation (which eventually leads to delayed emission) is somewhat less likely than in the larger QDs.

To learn more about the process of charge carrier separation, we measured the PL decay of the ensemble of QDs while dispersed in solvents of different refractive indices. Figure 3a shows how the decay dynamics change when going from a low refractive index (hexane; red; $n = 1.375$) to a high refractive index solvent (carbon disulfide; blue; $n = 1.627$). Solid lines are fits (see Methods). The average PL lifetime of the exciton becomes longer at lower refractive index (Figure 3b) because radiative decay is slower in a medium with lower refractive index, as described by the nanocrystal-cavity model.[29] From the data of Figure 3b, we estimate that the emissive QDs in the ensemble have a quantum efficiency of direct exciton emission around 80−90% (see Methods). We conclude that the decay of the emissive QDs is predominantly radiative, and accelerates with increasing solvent refractive index. The remaining 10−20% of the direct exciton decay may in large part be due to the charge-carrier separation process that gives rise to delayed emission eventually. Note that our photonic method yields the average quantum efficiency of the emissive quantum dots in the ensemble not including the dark fraction.[30]

Figure 3c shows that the relative contribution of the delayed component as a percentage of the total emission intensity is lower if the refractive index of the solvent is higher. This is the result of competition between charge carrier separation and direct exciton emission from the same excited state. If in a high refractive index solvent the rate of radiative decay from the exciton state is enhanced, then the probability of separation is reduced.[31] Hence, we must conclude that charge carrier separation occurs from the lowest-energy exciton state of our QDs (i.e., the emitting one), not from hot carrier states as previously proposed to explain so-called B-type blinking.[14] In fact, our model presented below provides an alternative but natural explanation for B-type blinking[14] (see Supporting Information, Figure S3).

Monte Carlo Simulation of Blinking and Delayed Emission. The similarity in power-law statistics for blinking

DOI: 10.1021/acs.nanolett.5b03818
Nano Lett. 2015, 15, 7718−7725

(Figure 1f) and delayed emission (Figure 2b) suggests that the same physical process underlies the two phenomena. Can delayed emission be explained in terms of existing models for blinking?[2] A model for blinking must at least contain (1) an explanation for the power-law statistics of ON and OFF durations and (2) a microscopic picture for the dark state. On the basis of the early paper of Efros and Rosen,[4] most models are "charging models" (Figure 4a). They ascribe the dark periods to temporary charging of the QD. In the charged state, emission is quenched, presumably by Auger recombination (step A in Figure 4a). Alternative "recombination center models"[11,12] propose that the QD becomes dark when fluctuations in the QD structure open and close the access to recombination centers that enable nonradiative recombination.

Only models based on charging are consistent with the observation of delayed emission on time scales from 100 ns to 1 ms (Figure 2b). Indeed, the observation of delayed emission implies that the QD can restore its emissive excited state milliseconds after initial excitation, which requires a long-lived metastable electronically excited state only present in charging models[5−7] (highlighted in Figure 4a). In existing charging models for blinking, this is a long-lived charge-separated state with one delocalized and one trapped charge. The release rates for the trapped charge fluctuate widely in time to explain the power-law distribution in OFF durations (Figure 1d). These wide fluctuations would also lead to power-law decay of the delayed emission (Figure 2b). We therefore conclude that our observation of delayed emission over long time scales supports a charging model for blinking, involving long-lived charge-separated states.

Recently, in specially designed core−shell structures a "gray state" with 10−40% intensity has been often observed in the blinking traces. It could be identified as a negatively charged state[15,33] with exponential blinking statistics[14,34] rather than power-law. The dynamics of this gray state are consistent with those of the negative trion state created electrochemically[14,35] or photochemically.[36] However, in most QDs a dark state (rather than a gray state) is dominant in the blinking trace. This darkest state (which comes with power-law statistics[34]) has recently been proposed by Park et al.[32] to involve ejection and trapping of an electron, leaving the QD with an excess positive charge in the valence band. We therefore tentatively identify the trapped charge in the charge-separated state involved in power-law blinking and delayed emission as the electron (as depicted in Figure 4a). Indeed, positive trions (consisting of an exciton plus the excess hole) created in the charge-separated dark state exhibit much faster Auger decay than negative trions involved in the gray state,[32,36] explaining that the charge-separated state is dark. This assignment is consistent with the conclusion in ref 18 that in Cu^+-doped CdSe the hole is always rapidly trapped on a Cu-center, while temporary trapping of the electron gives rise to delayed emission on millisecond time scales. To explain apparent discrepancies at the single-QD level between the decay rate of the dark state in blinking and the biexciton decay rate in CdSe QDs,[9] one might assume that the excess hole localizes at a defect or surface site. Indeed, also localized charge carriers can enable rapid Auger quenching.[37]

At first sight, delayed emission seems to fit in existing charging models for blinking, which propose long-lived charge-separated states.[5−7] There is however one important feature of delayed emission that is not properly accounted for in existing models, namely that the integrated intensity amounts to as much as 10−15% of the total emission. The models explain the long ON times that occur (see Figure 1f) in terms of unperturbed optical cycling (processes X,E in Figure 4a). In these models charge carrier separation is sometimes prevented for long periods, for example, by fluctuating tunnelling barriers and heights,[5] or Coulomb blockade.[6] As an example, in the diffusion model for blinking[7] the transition to a charge-separated state can be inaccessible for seconds if the configuration of the QD (parametrized by the coordinate Q in ref 7) diffuses away from the point where charge separation or release occurs. Although the statistics of blinking on time scales from microseconds to seconds were reported to be consistent with this model,[38] our observation of delayed emission is not. Indeed, if optical cycling went unperturbed for milliseconds or even seconds as existing models suggest, the relative contribution of the delayed emission could never become 10−15% of the total emission (see Supporting Information, Figure S4).

We have developed a simple model (Figure 4a) for blinking that simultaneously explains the (power-law distributed) ON and OFF durations of seconds in the intensity trace of a single QD (Figure 1c), and the significant contribution of delayed emission to the total emission (Figure 2b). In its simplest form, the model assumes a single trap that can cause charge separation by trapping an excited charge carrier, rendering the QD dark due to Auger quenching by the remaining carrier. The key ingredients of the model are that (1) the probability of charge carrier separation is fixed at a few percent (determined by competition with radiative decay; Figure 3), that (2) the exciton recovery rate is constant only during a power-law distributed time T, and that (3) after time T the recovery rate changes to a random new value such that the time-averaged distribution of recovery rates follows a power-law.[5−7] Power-law distributed times T would naturally follow from a microscopic picture that charge separation involves charge carrier trapping on a structural defect or a particular arrangement of the organic ligand shell and that energetic barriers for structural changes are exponentially distributed. For details of the model, see the Methods section.

The most radical difference with existing blinking models is the proposal here that at all times there is a finite probability of charge separation (which we assume fixed, but it can also be allowed to fluctuate around some mean value). This assumption ensures that the delayed emission has a sufficiently high integrated intensity and is supported by our finding that the contribution of delayed emission increases with decreasing refractive index (Figure 3). However, the assumption implies that long ON periods are in fact not characterized by unperturbed optical cycling, as currently assumed (compare Figure 4b,c). Hence, while in existing models periods of uninterrupted optical cycling can last from nanoseconds to many seconds[5−7] (Figure 4b), in our model they last for at most a few optical cycles (i.e., typically 1−10 μs in single-QD experiments). In our model, long "effectively ON" periods occur when for a long period T the exciton recovery rate is much faster than the excitation rate (~0.3 μs^{-1} in Figure 1e−h). In other words, such a period can last for seconds if the QD remains in a configuration such that trapped charge carriers are very rapidly released. The QD is then effectively ON, that is, optical cycling is interrupted by OFF periods so short (ns to μs) that they do not affect the emission intensity during period T (Figure 4c). Note that these short OFF periods are however responsible for the delayed emission that we observe in the PL decay traces of single QDs (Figure 1h and Supporting

DOI: 10.1021/acs.nanolett.5b03818
Nano Lett. 2015, 15, 7718−7725

Information, Figure S2). Interrupted optical cycling could also explain B-type blinking as observed by Galland et al.,[14] if we assume that the QDs examined have a (nearby) charge carrier trap with a release rate of approximately 10^4 s^{-1} (see Supporting Information, Figure S3) that switches between active and inactive. Such a trap may be introduced for example by the electrode used.

Figure 4d–f presents the results of a Monte Carlo simulation of the emission dynamics in a QD using our model. The intensity trace (Figure 4d) and distributions of ON and OFF durations (Figure 4e) are as typically encountered for single QDs. At the same time, the PL decay curve (Figure 4f) contains a power-law delayed component with a relative contribution of 15%. Hence, our new model successfully reproduces the most important aspects of the emission dynamics of QDs.

Charge carrier traps are usually associated with the surface of QDs, where the coordination of ions is incomplete. As a result, one might expect that charge carrier trapping in CdSe QDs would be reduced by the growth of a thicker protective CdS shell. Our measurements on CdSe/CdS QDs with different shell thicknesses reveal that the trend is exactly opposite to this expectation. Figure 5a shows the PL decay dynamics of CdSe/CdS core–shell QDs with shell thicknesses of 1 monolayer (blue), 6 monolayers (red), and 10 monolayers (green) on a time scale up to 10 μs after excitation. Solid lines are fits to eq 2, which yield the contribution P_S of delayed emission to the total emission. The fit results, presented in Figure 5b, reveal the trend that the delayed contribution (and hence the probability of charge carrier trapping) is larger for QDs with a thicker shell.

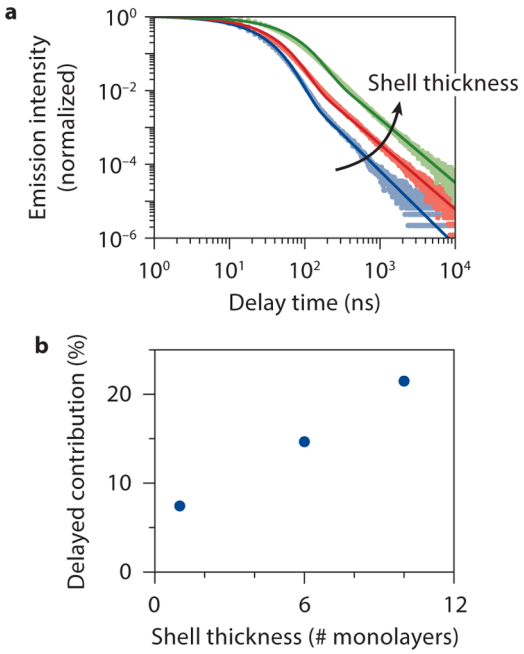

Figure 5. Delayed emission from quantum dots with different shell thicknesses. (a) PL decay curves from CdSe/CdS core–shell QDs with shell thicknesses of 1 monolayer (blue), 6 monolayers (red), and 10 monolayers (green), dispersed in toluene. The solid lines are fits to our model of direct exciton emission with exponential dynamics followed by a power-law delayed component (eq 2). (b) The contribution of delayed emission to the total emission of CdSe/CdS core–shell QDs as a function of shell thickness.

Figure 5 suggests that the charge carrier traps responsible for delayed emission are not located on the outer surface of the QD. The number of surface traps would presumably grow quadratically with shell size (proportional to the surface area) but the coupling strength to traps would become weaker exponentially (proportional to wave function overlap with core-localized states). Hence, an overall decrease in the effect of surface traps is expected with increasing shell thickness. Instead, the data presented in Figure 5 suggest that the charge carrier traps may in fact be situated in the CdS shell or on the core–shell interface. The charge carrier trapping can be more probable for thicker shells for several reasons: because there is a larger average number of traps per QD, because the electron wave function delocalizes more into the shell, or because strain at the core–shell interface is higher. The idea that the effect of charge carrier traps becomes more important with increasing CdS shell thickness is consistent with the finding of Bae et al.[39] that the quantum yield of an ensemble of CdSe/CdS core–shell QDs can in fact be lower for thicker shells. Furthermore, Nasilowski et al.[40] have recently measured that the PL dynamics in giant-shell QDs (>40 nm diameter) are completely dominated by very slow (μs) decay, which would be consistent with a major influence of temporary charge carrier trapping. The growth of a CdS shell, although a successful method to suppress Auger losses, seems to introduce additional (undesired) charge carrier traps in QDs. The challenge is to design new synthesis routes leading to superior CdS shells, yielding QDs with low Auger losses as well as few charge carrier traps.

Conclusion. To summarize, we have observed delayed emission from semiconductor QDs as direct evidence for the existence of a charge-separated state that recovers on time scales of nanoseconds to milliseconds. Charge separation takes place from the lowest exciton state, and the charge-separated state recovers to the lowest exciton state before emitting a delayed photon. The delayed emission exhibits power-law statistics very similar to those of the durations of bright and dark periods in blinking, suggesting a common origin. Indeed, we have successfully reproduced the delayed emission and the blinking statistics with a new blinking model, realizing that there is in fact no uninterrupted optical cycling during bright periods. The power-law distribution of exciton recovery rates implies that charge-separated states have lifetimes ranging from microseconds to seconds. Short-living charge-separated states (μs) hardly affect the brightness of the QD, as long as the excitation rate is slower than the exciton recovery rate. Efforts should mainly be aimed at reducing the effect of long-living charge-separated states (ms to s) because these lead to blinking and a resulting reduction in overall time-averaged brightness of the QD.

Methods. *Single Quantum Dot Spectroscopy.* For single-QD measurements, the QDs were spin coated on a HMDS (hexamethyl disilazane) coated borosilicate glass coverslip from a dilute dispersion in toluene and protected with a layer of spin-coated PMMA (poly(methyl methacrylate)). Single QDs were excited with supercontinuum light source (Fianium SC450) at a repetition rate of 1 MHz and a fluence of ~10^{-4} J/cm^2. The excitation wavelength of 532 nm was selected by spectral filtering using an acousto-optical tunable filter (Crystal Technologies) and an additional short pass filter. Fluorescence light was collected through the same objective used for excitation and separated from laser reflections using a long-pass filter with a cutoff at 590 nm. We used a Hanbury Brown-Twiss setup with two ID Quantique id100–20 ULN avalanche photodiodes (APDs; dark counts <10 Hz) connected to a

DOI: 10.1021/acs.nanolett.5b03818
Nano Lett. 2015, 15, 7718–7725

timing card (DPC 230, Becker & Hickl GmbH) with 165 ps time resolution.

Monte Carlo Simulation of the Emission Dynamics in a QD. The Monte Carlo simulation yielding the results of Figure 4 is done as follows. First the initial state of the trap is set, that is, the recovery rate γ_R and the "stationary time" T until diffusion to a new state. A recovery rate is generated from a power-law distribution with exponent α_R = 1.55, a low-end cutoff of 1/10 s and a high-end cutoff of 1/60 ns (see Supporting Information, Figure S1). The stationary time is generated by first generating a trap diffusion rate γ_D from a power-law distribution with exponent α_D = 1.7, a low-end cutoff of 1/10 s and a high-end cutoff of 1/60 ns, and then T from an exponential distribution with decay constant γ_D. The QD is excited every 1 μs for a period of 5 min. Following each excitation, there is a probability of P_S = 15% for charge carrier separation by trapping. If there is no separation (i.e., there is direct exciton recombination), a delay time t is simulated from an exponential distribution with decay constant $\gamma_X = 1/30$ ns. If there is separation, the actual recovery rate γ_R is used to generate from an exponential distribution the time t until recovery of the delocalized exciton state and delayed emission. Optical cycling does not proceed until after the trapped carrier is released. When the stationary time T is exceeded, the trap state is reset by generating a new recovery rate γ_R and a new stationary time T as described above.

Fitting Delayed Emission Dynamics. The normalized decay function due to a distribution of decay rates $\rho(\gamma) = \gamma^{\alpha-2}$ with an upper limit of γ_{max} is

$$I_d(t) = \int_0^{\gamma_{max}} \gamma\rho(\gamma)\mathrm{d}\gamma = \frac{\alpha-1}{\gamma_{max}^{\alpha-1}} t^{-\alpha}[\Gamma(\alpha) - \Gamma(\alpha, \gamma_{max}t)] \tag{1}$$

where $\Gamma(s)$ is the Gamma function, and $\Gamma(s, x)$ the incomplete Gamma function. Equation 1 describes power-law decay $I_d = t^{-\alpha}$ at long delay times $t \gg 1/\gamma_{max}$, while the factor between square brackets is a correction to keep the function well-behaved at short times $t \approx 0$. In Supporting Information Figure S1, we show that eq 1 with $\gamma_{max} = \gamma_X/2$ (where γ_X is the exciton decay rate) can be used as a good approximation for the delayed emission in case of back and forth charge separation and recovery of the exciton state. To fit the complete PL decay dynamics, we use a model function with one (Figure 4d) or two (Figure 3a) components of the form

$$I(t) = (1-P_S)\gamma_X e^{-\gamma_X t} + P_S \frac{\alpha-1}{(\gamma_X/2)^{\alpha-1}} t^{-\alpha} \times [\Gamma(\alpha) - \Gamma(\alpha, \gamma_X t/2)] \tag{2}$$

The first term is the exponential contribution due to direct exciton recombination. The second term is the delayed contribution. In Supporting Information Figure S1, we explain that P_S must be interpreted as the probability of charge carrier separation for times longer than the intrinsic exciton lifetime $\tau_X = 1/\gamma_X$.

Estimating the PL Quantum Efficiency with the Nanocrystal-Cavity Model. The rate of radiative decay γ_{rad} scales linearly with the local density of optical states experienced by an emitter. In a nanocrystal the local density of optical states depends on the refractive index of the surrounding solvent n, as described by the nanocrystal-cavity model[29]

$$\gamma_{rad} \propto n\left(\frac{3n^2}{2n^2 + n_{NC}^2}\right)^2 \tag{3}$$

Here n_{NC} is the refractive index of the nanocrystal. We take n_{NC} = 2.5, which is the refractive index for CdS around 600 nm[41] (see Supporting Information, Figure S6 for a discussion). A local-field correction factor, as appears in eq 3, has previously been taken into account to calculate the transition rates[25,28] and absorption strengths[42,43] of QDs in a particular solvent.

The experimental exciton lifetimes τ_X as a function of refractive index (Figure 3b) are determined by a refractive-index dependent radiative component and a (presumably) fixed nonradiative component. We fit the data to

$$\tau_X = \left[An\left(\frac{3n^2}{2n^2 + n_{NC}^2}\right)^2 + B\right]^{-1} \tag{4}$$

where the first term describes radiative decay (parametrized by the parameter A), and the second term is the nonradiative decay rate B (including the charge carrier separation rate). Using the fitted values of A and B the PL quantum efficiency $\eta(n)$ is calculated as

$$\eta(n) = 1 - B\left[An\left(\frac{3n^2}{2n^2 + n_{NC}^2}\right)^2 + B\right]^{-1} \tag{5}$$

The solvents used are hexane (n = 1.375), cyclohexane (n = 1.426), chloroform (n = 1.444), trichloroethylene (n = 1.478), toluene (n = 1.496), chlorobenzene (n = 1.524), and carbon disulfide (n = 1.627).

Fitting Emission Spectra to a Two-Sided Gaussian. The emission spectra of Figures 2c,d have an asymmetric shape, determined by the distribution of sizes and shapes in the ensemble. To fit the peak positions and band widths, we use two-sided Gaussian functions on energy (rather than wavelength) scale

$$I(E) = A\begin{cases} e^{-(E-E_0)^2/2\sigma_1^2}; & E < E_0 \\ e^{-(E-E_0)^2/2\sigma_2^2}; & E > E_0 \end{cases} \tag{6}$$

where A is the amplitude, E_0 is the peak energy, σ_1 is the width on the red side, and σ_2 is the width on the blue side of the spectrum. In Figure 2e, we plot the peak positions E_0 and the full widths at half-maximum $\sqrt{2\ln 2}\,(\sigma_1 + \sigma_2)$ of the emission spectra.

■ ASSOCIATED CONTENT

Supporting Information

The Supporting Information is available free of charge on the ACS Publications website at DOI: 10.1021/acs.nanolett.5b03818.

Synthesis procedure of the core−multishell QDs examined; derivation of eq 2, which describes photoluminescence decay dynamics including delayed emission; examples of delayed emission measured on individual quantum dots; discussion of B-type blinking in terms of our new blinking model; discussion of what existing blinking models would predict for the delayed contribution; threshold analysis of the blinking trace of Figure 1e; and analysis of how the refractive index of the

DOI: 10.1021/acs.nanolett.5b03818
Nano Lett. 2015, 15, 7718−7725

quantum dots affects the results from the nanocrystal-cavity model. (PDF)

AUTHOR INFORMATION

Corresponding Author

*E-mail: d.vanmaekelbergh@uu.nl.

Notes

The authors declare no competing financial interest.

ACKNOWLEDGMENTS

This work is part of the research program of the "Stichting voor Fundamenteel Onderzoek der Materie (FOM)", which is financially supported by the "Nederlandse Organisatie voor Wetenschappelijk Onderzoek (NWO)" (programs 131 "Light Management in New Photovoltaic Materials", FP/AV-09.0224 "Functional Nanoparticle Solids", and 13DDC01 "Designing Dirac Carriers in Semiconductor Superstructures"). Support from the U.S. NSF (DMR-1206221 to DRG) is acknowledged.

REFERENCES

(1) Frantsuzov, P.; Kuno, M.; Jankó, B.; Marcus, R. A. *Nat. Phys.* **2008**, *4*, 519−522.
(2) Cordones, A. A.; Leone, S. R. *Chem. Soc. Rev.* **2013**, *42*, 3209−3221.
(3) Nirmal, M.; Dabbousi, B. O.; Bawendi, M. G.; Macklin, J. J.; Trautman, J. K.; Harris, T. D.; Brus, L. E. *Nature* **1996**, *383*, 802−804.
(4) Efros, Al. L.; Rosen, M. *Phys. Rev. Lett.* **1997**, *78*, 1110−1113.
(5) Kuno, M.; Fromm, D. P.; Hamann, H. F.; Gallagher, A.; Nesbitt, D. J. *J. Chem. Phys.* **2001**, *115*, 1028−1040.
(6) Verberk, R.; Van Oijen, A. M.; Orrit, M. *Phys. Rev. B: Condens. Matter Mater. Phys.* **2002**, *66*, 233202.
(7) Tang, J.; Marcus, R. A. *J. Chem. Phys.* **2005**, *123*, 054704.
(8) Rosen, S.; Schwartz, O.; Oron, D. *Phys. Rev. Lett.* **2010**, *104*, 157404.
(9) Zhao, J.; Nair, G.; Fisher, B. R.; Bawendi, M. G. *Phys. Rev. Lett.* **2010**, *104*, 157403.
(10) Cordones, A. A.; Bixby, T. J.; Leone, S. R. *Nano Lett.* **2011**, *11*, 3366−3369.
(11) Frantsuzov, P. A.; Marcus, R. A. *Phys. Rev. B: Condens. Matter Mater. Phys.* **2005**, *72*, 155321.
(12) Frantsuzov, P. A.; Volkán-Kacsó, S.; Jankó, B. *Phys. Rev. Lett.* **2009**, *103*, 207402.
(13) Frantsuzov, P. A.; Volkán-Kacsó, S.; Jankó, B. *Nano Lett.* **2013**, *13*, 402−408.
(14) Galland, C.; Ghosh, Y.; Steinbrück, A.; Sykora, M.; Hollingsworth, J. A.; Klimov, V. I.; Htoon, H. *Nature* **2011**, *479*, 203−207.
(15) Qin, W.; Guyot-Sionnest, P. *ACS Nano* **2012**, *6*, 9125−9132.
(16) Sher, P. H.; Smith, J. M.; Dalgarno, P. A.; Warburton, R. J.; Chen, X.; Dobson, P. J.; Daniels, S. M.; Pickett, N. L.; O'Brien, P. *Appl. Phys. Lett.* **2008**, *92*, 101111.
(17) Jones, M.; Lo, S. S.; Scholes, G. D. *Proc. Natl. Acad. Sci. U. S. A.* **2009**, *106*, 3011−3016.
(18) Whitham, P. J.; Knowles, K. E.; Reid, P. J.; Gamelin, D. R. *Nano Lett.* **2015**, *15*, 4045−4051.
(19) De Mello Donegá, C. *Chem. Soc. Rev.* **2011**, *40*, 1512−1546.
(20) Grabovskis, V. Ya.; Dzenis, Ya. Ya.; Ekimov, A. I.; Kudryavtsev, I. A.; Tolstoi, M. N.; Rogulis, U. T. *Sov. Phys. Solid State* **1989**, *31*, 149−151.
(21) Bharadwaj, P.; Novotny, L. *Nano Lett.* **2011**, *11*, 2137−2141.
(22) Gómez, D. E.; Van Embden, J.; Mulvaney, P.; Fernée, M. J.; Rubinsztein-Dunlop, H. *ACS Nano* **2009**, *3*, 2281−2287.
(23) Spinicelli, P.; Buil, S.; Quélin, X.; Mahler, B.; Dubertret, B.; Hermier, J.-P. *Phys. Rev. Lett.* **2009**, *102*, 136801.
(24) Galland, C.; Ghosh, Y.; Steinbrück, A.; Hollingsworth, J. A.; Htoon, H.; Klimov, V. I. *Nat. Commun.* **2012**, *3*, 908.
(25) Efros, Al. L.; Rosen, M.; Kuno, M.; Nirmal, M.; Norris, D. J.; Bawendi, M. *Phys. Rev. B: Condens. Matter Mater. Phys.* **1996**, *54*, 4843−4856.
(26) Delerue, C.; Lannoo, M. *Nanostructures − Theory and Modelling*; Springer-Verlag: Berlin, 2004; p 149.
(27) Van Driel, A. F.; Allan, G.; Delerue, C.; Lodahl, P.; Vos, W. L.; Vanmaekelbergh, D. *Phys. Rev. Lett.* **2005**, *95*, 236804.
(28) Liu, H.; Guyot-Sionnest, P. *J. Phys. Chem. C* **2010**, *114*, 14860−14863.
(29) Senden, T.; Rabouw, F. T.; Meijerink, A. *ACS Nano* **2015**, *9*, 1801−1808.
(30) Würth, C.; Geißler, D.; Behnke, T.; Kaiser, M.; Resch-Genger, U. *Anal. Bioanal. Chem.* **2015**, *407*, 59−78.
(31) Rabouw, F. T.; Den Hartog, S. A.; Senden, T.; Meijerink, A. *Nat. Commun.* **2014**, *5*, 3610.
(32) Park, Y. S.; Bae, W. K.; Pietryga, J. M.; Klimov, V. I. *ACS Nano* **2014**, *8*, 7288−7296.
(33) Javaux, C.; Mahler, B.; Dubertret, B.; Shabaev, A.; Rodina, A. V.; Efros, A. L.; Yakovlev, D. R.; Liu, F.; Bayer, M.; Camps, G.; Biadala, L.; Buil, S.; Quélin, X.; Hermier, J.-P. *Nat. Nanotechnol.* **2013**, *8*, 206−212.
(34) Rabouw, F. T.; Lunnemann, P.; Van Dijk-Moes, R. J. A.; Frimmer, M.; Pietra, F.; Koenderink, A. F.; Vanmaekelbergh, D. *Nano Lett.* **2013**, *13*, 4884−4892.
(35) Jha, P. P.; Guyot-Sionnest, P. *ACS Nano* **2009**, *3*, 1011−1015.
(36) Cohn, A. W.; Rinehart, J. D.; Schimpf, A. M.; Weaver, A. L.; Gamelin, D. R. *Nano Lett.* **2014**, *14*, 353−358.
(37) Cohn, A. W.; Schimpf, A. M.; Gunthardt, C. E.; Gamelin, D. R. *Nano Lett.* **2013**, *13*, 1810−1815.
(38) Pelton, M.; Smith, G.; Scherer, N. F.; Marcus, R. A. *Proc. Natl. Acad. Sci. U. S. A.* **2007**, *104*, 14249−14254.
(39) Bae, W. K.; Padilha, L. A.; Park, Y.-S.; McDaniel, H.; Robel, I.; Pietryga, J. M.; Klimov, V. I. *ACS Nano* **2013**, *7*, 3411−3419.
(40) Nasilowski, M.; Spinicelli, P.; Patriarche, G.; Dubertret, B. *Nano Lett.* **2015**, *15*, 3953−3958.
(41) Jensen, B.; Torabit, A. *J. Opt. Soc. Am. B* **1986**, *3*, 857−863.
(42) Leatherdale, C. A.; Woo, W.-K.; Mikulec, F. V.; Bawendi, M. G. *J. Phys. Chem. B* **2002**, *106*, 7619−7622.
(43) Moreels, I.; Lambert, K.; Smeets, D.; De Muynck, D.; Nollet, T.; Martins, J. C.; Vanhaecke, F.; Vantomme, A.; Delerue, C.; Allan, G.; Hens, Z. *ACS Nano* **2009**, *3*, 3023−3030.

DOI: 10.1021/acs.nanolett.5b03818
Nano Lett. 2015, 15, 7718−7725